Geldanamycin treatment does not result in anti-cancer activity in a preclinical model of orthotopic mesothelioma

M. Lizeth Orozco Morales[1,2,3], Catherine A. Rinaldi[1,2,4], Emma de Jong[5], Sally M. Lansley[3], Y. C. Gary Lee[3], Rachael M. Zemek[5], Anthony Bosco[5], Richard A. Lake[1,2.3], W. Joost Lesterhuis*[1,2,3,5]

[1]School of Biomedical Sciences, University of Western Australia, Crawley, WA 6009, Australia

[2]National Centre for Asbestos Related Diseases, Nedlands, WA 6009, Australia

[3]Institute for Respiratory Health, Nedlands, WA 6009, Australia

[4]Centre for Microscopy Characterisation and Analysis, Nedlands, WA 6009, Australia

[5]Telethon Kids Institute, The University of Western Australia, Nedlands, WA 6009, Australia

*Corresponding author and lead contact: W. Joost Lesterhuis, willem.lesterhuis@uwa.edu.au

ABSTRACT

Mesothelioma is characterised by its aggressive invasive behaviour, affecting the surrounding tissues of the pleura or peritoneum. We compared an invasive pleural model with a non-invasive subcutaneous model of mesothelioma and performed transcriptomic analyses on the tumour samples. Invasive pleural tumours were characterised by a transcriptomic signature enriched for genes associated with MEF2C and MYOCD signaling, muscle differentiation and myogenesis. Further analysis using the CMap and LINCS databases identified geldanamycin as a potential antagonist of this signature, so we evaluated its potential *in vitro* and *in vivo.* Nanomolar concentrations of geldanamycin significantly reduced cell growth, invasion, and migration *in vitro*. However, administration of geldanamycin *in vivo* did not result in significant anti-cancer activity. Our findings show that myogenesis and muscle differentiation pathways are upregulated in pleural mesothelioma which may be related to the invasive behaviour. However, geldanamycin as a single agent does not appear to be a viable treatment for mesothelioma.

INTRODUCTION

Mesothelioma is a cancer that usually arises in the pleura, occasionally developing from other serous membranes (1). Its development is associated with asbestos exposure, with a latency period of approximately 40 years between exposure and diagnosis (2). Mesothelioma's morbidity is predominantly caused by local invasion into neighbouring tissues such as lungs, heart, diaphragm, and chest wall (3). On a cellular level, local invasion is a coordinated process that requires the cancerous cells to interact with the tumour microenvironment, the cell matrix, or other cells as part of a cell-cell adhesion process (4), with several signalling pathways controlling these interactions, as well as the cytoskeletal dynamics in the tumour cells and the cell movement into adjacent tissues (5).

For many mesothelioma patients, palliative chemotherapy with cisplatin/pemetrexed is the first-line therapy (6). Recently, cancer immunotherapy with nivolumab plus ipilimumab improved overall survival in mesothelioma patients compared to cisplatin/pemetrexed (7). Combination immune-chemotherapy with anti-PD-L1 antibody durvalumab and cisplatin/pemetrexed showed a promising progression-free survival (8), which is now further explored in a randomized phase 3 trial (9). However, despite this progress, most patients still do not respond to these treatments.

Recent developments in systems biology have allowed gene expression profiling to be used not only for comparing specific pathology but also to unravel drug-disease associations (10). The connectivity map (CMap) dataset has been used as a systematic approach to connect gene expression profiles associated with disease with drug-induced expression profiles, and thereby identify drug repurposing candidates that are predicted to reverse or reinforce genomic signatures of disease (11). In addition, the library of integrated network-based signatures (LINCS) L1000 dataset, has over a million gene expression profiles from cell lines treated with small molecules, growth factors, cytokines and drugs. This allows potential identification of drugs that are predicted to mimic or reverse the input gene expression signature by comparing the LINCS L1000 datasets and disease-specific signatures (12). The expectation of this approach is that existing drugs with known safety profiles can be repurposed for alternative indications, accelerating the clinical development pathway (13).

Here, using transcriptomic data from invasive and non-invasive models of murine mesothelioma, we aimed to map an invasive signature of mesothelioma and identify drug repurposing candidates with potential anti-mesothelioma activity.

RESULTS

Muscle development and myogenesis signatures are associated with the invasive pleural mesothelioma model

By inoculating the same mesothelioma cell lines AB1 and AE17 in tandem, we have previously shown that mesothelioma cells grow significantly faster in the pleural space compared to the subcutaneous space (14). Additionally, we found that the intrapleural (IPL) tumour microenvironment induces or permits an invasive phenotype whereas the subcutaneous (SC) environment does not. We performed RNA sequencing of tumours from both the pleural and subcutaneous locations, while making sure only tumour was excised, not any surrounding normal tissue such as lung, heart, bone, or muscle (Fig 1A) (14). Differential expression analysis (15) identified 419 genes that were differentially expressed between the IPL and SC tumours in both AE17 (C57BL/6 background) and AB1 (BALB/c background) mesotheliomas. Ingenuity Pathway Analysis (16) of the differentially expressed genes showed the two most significant predicted upstream transcription factors as myocyte-specific enhancer factor 2C (MEF2C), which maintains the differentiated state of muscle cells during myogenesis (17) (p. value = 3.4×10^{-8}, z-score = 2.78) and myocardin (MYOCD), a co-transcriptional activator of serum response factor that inhibits the cell cycle and induces smooth muscle differentiation (18) (p. value = 1.5×10^{-5}, z-score = 2.96).

To determine which biological pathways were upregulated in the IPL tumours, we used InnateDB (19). This identified ten significant pathways from the Reactome and KEGG databases in both tumour models (p. value < 0.05) (Fig 1B). The most significant pathways were related to muscle contraction, cardiomyopathy and myogenesis. To determine the functional characteristics of the pleural invasion-related set of genes, we performed pre-ranked gene set enrichment analysis (GSEA) (20) (21). This identified nine gene sets from the gene ontology biological process consortium (22), and one gene set from the hallmark collection (23), that were consistently enriched in both invasive models (p. value < 0.05, false discovery rate (FDR) < 0.25, Fig 1C). These gene sets mainly related to muscle development, morphogenesis, and actin processes, and myogenesis, suggesting that muscle development signatures were related to the invasive phenotype of pleural mesothelioma.

Fig 1. Muscle development and myogenesis signatures are associated with the invasive pleural mesothelioma model (A) Experimental design, n (mice) = 8 per group. (B) Canonical pathways analysis of differentially expressed genes using InnateDB,

p values 0.05 and 0.01 are represented with dotted line on –log10 = 1.3 and 2, respectively. (C) GSEA of differentially expressed genes, between the pleural and subcutaneous tumours in both AB1 and AE17. Circle size represents number of significant genes, colour represents adjusted p value.

LINCS and CMap analyses identify geldanamycin as a potential inhibitor of mesothelioma invasion-related pathways

We went on to identify drug repurposing candidates that were predicted to target these mesothelioma invasion-associated pathways. We interrogated the LINCS L1000 Chem Pert repository (22) and the CMap database (11), accessed via the Enrichr platform (24) (25) (26), using the genes that were upregulated in the invasive (pleural) AB1 and AE17 mesothelioma models as input data. This analysis identified geldanamycin as the only drug to be significantly associated with the invasive signature in both databases (LINCS L1000; p value < 0.0001, CMAP; p. value = 0.012, Supplementary Data S1). Geldanamycin and its derivatives are inhibitors of heat-shock protein 90 (27) (28), and previous studies demonstrated significant inhibitory effects on myogenic differentiation and muscle regeneration (29) (30), as well as direct anti-cancer effects, including in mesothelioma *in vitro* (31) (32). Together, these results suggested that geldanamycin might have anti-cancer activity in pleural mesothelioma.

Low-nanomolar concentrations of geldanamycin inhibit mesothelioma cell growth, invasion, and migration *in vitro*

Having identified geldanamycin as a possible drug to target mesothelioma invasion, we tested its effect on cellular proliferation in the murine mesothelioma cell lines AB1, AE17, the human mesothelioma cell lines VGE62, JU77 and MSTO-211H, and the non-cancerous fibroblast murine cell line NIH3T3. This showed IC_{50} values at low-nanomolar concentration for all cell lines (Fig 2A - 2F). In

addition, we observed that geldanamycin significantly decreased JU77 growth in a soft agar colony formation assay at 6.25 nM concentration and higher (p. value < 0.0009; Fig 2G and 2H).

To evaluate the effect of geldanamycin on mesothelioma migration and invasion *in vitro* we employed scratch assays. Geldanamycin significantly inhibited migration (Fig 2I - 2L) and invasion in a concentration-dependent manner (Fig 2M - 2P).

Fig 2. Nanomolar concentrations of geldanamycin inhibit cancer cell growth, invasion, and migration *in vitro* (A to F) MTT assay in (A) AB1, (B) AE17, (C) NIH3T3, (D) VGE62, (E) MSTO-211H, and (F) JU77 cell lines. The curve is presented as a non-linear regression; log(geldanamycin) versus response. IC_{50} values are in nM. Data are presented as means ± SD of 3 replicates. (G and H); data are means ± SD of 3 replicates, unpaired t test was used to determine significance. Soft agar colony formation assay for JU77 human mesothelioma cell line. Geldanamycin was added at 100, 50, 25, 12.5, 6.25 nM and the control (0 nM). (G) Colony counting was performed using ImageJ software. Edges were excluded, size = $pixel^2$ 0 – infinity, circularity = 0.00 – 1.00. (I to L) Scratch assay for migration in (I) AB1, (J) AE17, (K) VGE62, and (L) NIH3T3 cell lines. Geldanamycin was serial diluted from 2000 nM to 3.9 nM, with 0 nM as control. Data are means of 3 replicates. (M to P) Scratch assay with matrigel at 8 mg/mL for invasion in (M) AB1, (N) AE17, (O) VGE62, and (P) NIH3T3 cell lines. Geldanamycin was serial diluted from 80 nM to 5 nM and 0 nM as control. Data are means of 3 replicates.

Geldanamycin treatment does not have anti-mesothelioma activity *in vivo*

To assess any therapeutic effect of geldanamycin on mesothelioma invasion and growth *in vivo,* we used our optimised model of orthotopic invasive mesothelioma (14). We inoculated AB1 cells expressing luciferase (AB1-Luc) intraperitoneally and administered geldanamycin twice daily for 5 days and monitored mesothelioma growth using bioluminescence imaging (Fig 3A). Optimization experiments showed that geldanamycin at a dose of 0.1 mg/kg was tolerable and did not result in any discomfort (Fig 3B, Fig S1A-B). This dose has previously been shown to result in a significant biological effect in vivo, in an oedema mouse model (33). There was no significant effect on tumour growth in the geldanamycin group when compared to vehicle controls (Fig 3C and 3D). To determine whether geldanamycin had any effect on mesothelioma invasion, we collected the tumours and surrounding

tissues for histological analysis. We found that geldanamycin did not affect mesotheliomas invasion, with both groups showing clear invasion of mesothelioma cells into the surrounding organs such as liver, intestine and pancreas (Fig 3E). Together, these data show that geldanamycin does not have any significant effect on the proliferation or invasion of mesothelioma *in vivo*.

Fig 3. Geldanamycin does not result in significant anti-mesothelioma activity *in vivo* (A) Experimental design. (B) Mice weight monitored daily during treatment. (C) Bioluminescence imaging for tumour bioluminescence monitoring on days 4, 7 and 10 for control group and geldanamycin group. (D) Tumour bioluminescence comparison based on average radiance ($p/s/cm^2/sr$) over time. Data are means ± SD values. n = 5. Unpaired t-test. (E) IP tumours were stained with hematoxylin and eosin. Blue arrows indicate tumour invasion in different organs. Scale bar = 100 µm.

DISCUSSION

Targeting invasion in the treatment of mesothelioma is of great interest, given the central role of invasion in the morbidity of this disease. Previous clinical studies have attempted to inhibit invasion in mesothelioma patients by targeting mesothelin (34) (35), a membrane-bound protein that stimulates anchorage-independent growth, migration, and invasion (36) (37). However, progression free survival was not different between the treatment and control groups. Another study (38) targeted the Met signalling pathway, a known mesothelioma invasion promoting pathway (39). However, no results have been reported to date.

In the present study, we aimed to identify regulators of mesothelioma invasion by comparing invasive intrapleural tumours with non-invasive subcutaneous tumours. Using transcriptomic data from these models, we identified MEF2C and MYOCD as upstream regulators of the invasive mesothelioma model. Altered MEF2C regulation has been implicated as driver of cancer development (40), and it acts as an oncogene for immature T-cell acute lymphoblastic leukaemia (41), myeloid leukaemia (42), hepatocellular carcinoma (43), and pancreatic ductal adenocarcinoma (44). Perturbations in MYOCD , are associated with heart failure, acute vessel disease, diabetes and cancer (45), with some MYOCD-

149 related transcription factors regulating cytoskeletal dynamics (46) which can benefit tumour migration
150 and invasion (47).

151 Using canonical pathway analysis and GSEA, we identified muscle development and myogenesis
152 signatures associated with the invasive model. Using the LINCS L1000 Chem Pert repository and the
153 CMap database, we identified geldanamycin, an antibiotic isolated from *Streptomyces hygroscopicus*
154 (48) and a naturally occurring benzoquinone ansamycin that targets Hsp90 (27), as a potential drug to
155 target these myogenesis and muscle differentiation signatures in invasive mesothelioma.
156 Geldanamycin has previously been shown to inhibit muscle regeneration and myogenic differentiation
157 (29) (30), and geldanamycin and its derivatives have been previously recognised as anti-cancer agents
158 (49). *In vitro* cancer studies in squamous cell carcinoma demonstrated significant inhibition of cell
159 proliferation and G2 arrest by geldanamycin (50), and it inhibited angiogenesis and invasion in a
160 prostate cancer model, mediated by the hypoxia-inducible factor 1α (51). Particularly for
161 mesothelioma, a study by Okamoto et al. (2008) showed that *in vitro* use of tanespimycin, a less-toxic
162 derivative of geldanamycin, led to significant G1 and G2/M cell cycle arrest and apoptosis, while
163 inhibiting cell proliferation in mesothelioma cells (52).

164 In our study, we also observed a significant reduction on tumour growth, cell migration and cell
165 invasion *in vitro,* with an IC_{50} in the nanomolar range for all the tested cell lines. However, the
166 metabolism and cell movement of the non-cancerous cell line NIH3T3 was significantly inhibited as
167 well, with an IC_{50} of 59 nM. This non-cancer selective inhibition could be related to the toxicity that
168 we observed *in vivo* when dosing geldanamycin at 1 and 0.5 mg/kg. Most importantly, we did not
169 observe any anti-mesothelioma activity for geldanamycin in an orthotopic model, when given at a
170 tolerable yet biologically active dose (33).

171 This lack of translation from *in vitro* to *in vivo* activity could be related to an insufficiently wide
172 therapeutic window, with tolerable drug exposure levels *in vivo* being too low to result in sufficient
173 anti-cancer effect as we observed *in vitro*. In addition, it is possible that compensatory mechanisms

are operational *in vivo* that allow the cancer cells to escape geldanamycin-induced anti-cancer effects. Alternatively, the myogenesis gene expression profile may be a bystander effect of exposure to the orthotopic environment, rather than a program driving invasive mesothelioma growth. Lastly, drug repurposing approaches have their limitations, in particular when based on an overlap in gene expression signatures between disease-associated tissues and cell lines treated with compounds, such as LINCS/CMap, resulting in false-positive hits (53) (54) (55). Other treatment avenues will need to be explored to specifically target mesothelioma invasion.

METHODS

Cell culture. Cell lines AE17 (56) and AB1 (57) were obtained from and verified by CellBank Australia. AB1 was transfected to express the luciferase (AB1-Luc) (58). Cell lines MSTO-211H and NIH3T3 were obtained from and verified by ATCC. Cell lines VGE62, JU77 were established in-house from pleural mesothelioma patients (59). AB1, AE17, VGE62, MSTO-211H, NIH3T3 and JU77 were maintained in complete R10 medium, RPMI 1640 (Invitrogen) supplemented with 10% foetal calf serum (FCS; Life Technologies), 20 mM HEPES (Sigma-Aldrich), 0.05 mM 2-mercaptoethanol (pH 7.2; Merck, Kilsyth, Australia), 60 µg/mL penicillin (Life Technologies), 50 µg/mL gentamicin (David Bull Labs). All cell lines were confirmed mycoplasma negative by polymerase chain reaction. All cells were cultured as a monolayer at 37 °C in a humidified atmosphere with 5% CO_2. Cells were passaged at approximately 1:10-1:5 every 2-3 days when reaching 75-80% confluence.

Mice. This study was conducted in accordance with the institutional guidelines of the Harry Perkins Institute of Medical Research Animal Ethics Committee (approvals AE057 and AE183). Female BALB/c and Female C57BL/6 mice were obtained from the Animal Resource Centre (Murdoch, WA, Australia). All mice were 8 to 12 weeks of age when used for the experiments. Mice were housed at the Harry Perkins Institute of Medical Research Bioresources Facility under pathogen-free conditions at 21 °C to 22 °C with a 12/12 h light cycle. Cages (Tecniplast) had an individual air filtered system and contained

aspen chips bedding (TAPVEI). Mice were fed Rat and Mouse cubes (Specialty Feeds) and had access to filtered water. Animal monitoring: mice were monitoring a minimum of twice weekly prior to the start of the experiment. Following ip tumour inoculation, clinical score and welfare points (Supplementary Table S1 and S2) were closely followed to ensure animals were well. Mice were monitored the day after inoculation and daily monitored from day one of treatment (day 4 after inoculation) until end of experiment (day 10 after inoculation). Weight was recorded prior to first treatment injection and all mice were weighed daily during treatment. If weight dropped more than 10% mice stopped receiving treatment until recovered. Tumour size was measured using IVIS (See below: In vivo imaging system (IVIS)). The endpoint was selected based on treatment schedule (finishing on day 10) as opposed to waiting for clinical signs to appear.

Tumour cell inoculation. Cells were trypsinized and washed two times in phosphate buffer saline (PBS) and counted with trypan blue dye. For the SC tumour model, mice were shaved on the right-hand flank and inoculated with 5 x 10^5 AB1 or 1 x 10^6 AE17 cells suspended in 100 µL PBS. Tumour volume (mm^3) was monitored with callipers. For the IPL tumour model, mice were anaesthetised under continuous isofluorane and inoculated with 5 x 10^5 AB1 or 1 x 10^6 AE17 cells suspended in 200 µL PBS into the pleural space as previously described (60). For the IP tumour model, mice where inoculated in the intraperitoneal cavity on the right flank with 5 x 10^5 AB1-Luc cells suspended in 200 µL PBS. Tumour size was determined by in vivo imaging system, see below. All mice were euthanized in accordance with animal ethics guidelines.

Tumour preparation for RNA sequencing. At day 10 after tumour inoculation, mice were euthanized and the tumours were harvested and submerged in RNAlater (Life Technologies) at 4 °C overnight to allow RNAlater to penetrate the tissue. Then, tumours were removed from RNAlater and stored at –80 °C until dissociation with TRIzol (Life Technologies) using a TissueRuptor (QIAGEN). RNA was extracted with chloroform and purified on RNeasy MinElute columns (QIAGEN).

RNA sequencing analysis. Library preparation and sequencing at 50 bp single end reads with Illumina HiSeq standard protocols were performed by Australian Genome Research Facility.

Alignment was performed using Kallisto (61). Differentially expressed genes were identified between IPL and SC tumours within both AB1 and AE17 models using DESeq2 (15). P values were adjusted for multiple comparisons using the Benjamini–Hochberg (B-H) method. A p value < 0.05 was considered significant. Differentially expressed genes were analysed as follows: Ingenuity Systems (16) was used to identify predicted upstream regulators, using right-tailed Fisher's exact tests and default settings for other options; activation Z-scores were calculated for each regulator by comparing their known effect on downstream targets with observed changes in gene expression. Those with activation Z-scores ≥2 or ≤2 were considered "activated" or "inhibited", respectively. Pathways analysis from InnateDB (62) (19) was used to identify relevant canonical pathways. Enrichment analysis was performed with Enrichr (24) (25) (26). LINCS L1000 Chem Pert repository (22) and CMap (11) were used to identify drugs that were predicted to phenocopy our gene expression profile of interest (P value < 0.05). Pre-ranked GSEA (20) (21) was used to identify enriched gene sets from the gene ontology (22) and hallmark (23) consortiums; p. value < 0.05 and FDR < 0.25 were considered significant.

Soft agar colony formation. Cells were incubated with different concentrations of geldanamycin (100, 50, 25, 12.5 6.25 and 0 nM) for a soft agar colony formation assay (63). Briefly, 3% 2-hydroxyethyl agarose (agarose, A4018; Sigma-Aldrich, Australia) was prepared as stock solution. The bottom layer was prepared by incubating 20% agarose gel in R10 complete medium, RPMI 1640 (Invitrogen) supplemented with 10% foetal calf serum (FCS; Life Technologies), 20 mM HEPES (Sigma-Aldrich), 0.05 mM 2-mercaptoethanol (pH 7.2; Merck, Kilsyth, Australia), 60 µg/mL penicillin (Life Technologies), 50 µg/mL gentamicin (David Bull Labs), for a final concentration of 0.6%, 2mL per well, at 4 °C for 1 h to allow the mixture to solidify, then incubating at 37 °C for at least 30 min before seeding the cells. The cell-containing layer (10% agarose gel in R10 complete medium for a final concentration of 0.3%, 1 mL

per well) was prepared with a concentration of 1,000 cells/mL. 1 mL of cells was then transfer to each well. The feeder layer (10% agarose gel in R10 complete medium for a final concentration of 0.3%, 1 mL per well was prepared with different concentrations of geldanamycin; each different concentration was then added to each well on top of the cells. The 6-well plate was then incubated at 4 °C for 15 min before incubating at 37 °C with 5% CO_2 for a week. A new feeder layer was added once per week until day 22.

Colony counting was performed by adding 1 mL of 0.005% crystal violet (C0775; Sigma-Aldrich, Australia) in PBS on top of each well and incubating at room temperature for 24 h. Pictures were taken and colonies counted with ImageJ (v1.52a).

Migration and matrigel invasion assay. Cells were harvested and seeded in Incucyte ImageLock 96-well plates (Essen BioScience) at a density of 10 x 10^4 cells/mL overnight. A scratch wound was performed on the confluent cells with the 96-pin IncuCyte WoundMaker Tool (Essen BioScience). For migration assays, cells were washed with PBS once before adding 100 µL media with geldanamycin at indicated concentrations. For matrigel invasion assays, cells were washed with PBS once before adding 50 µL of matrigel basement membrane matrix (FAL356231; Corning, NY, USA) at 8 mg/mL. Lastly, 100 µL media with geldanamycin at indicated concentrations were added on top of the matrigel. Cells were incubated in the IncuCyte ZOOM at 37 °C with 5% CO_2 and pictures were taken every 2 hours. Data were analysed using the Incucyte Scratch Wound Cell Migration Software Module, calculating the Relative Wound Density (%) (RWD) for both migration and invasion assays.

MTT assay. Cells were harvested and seeded in 96-flat well plates (Corning) at a density of 5 x 10^4 cells/mL overnight. Media was removed and 100 µL media with geldanamycin at indicated concentrations was added to each well. Cell viability and toxicity were measured at 48 h. Cells were incubated with 50 µL of a 2 mg/mL solution of (3-(4,5-dimethyl-thiazole-2-yl)-2,5-biphenyl tetrazolium (MTT, Sigma-Aldrich) in PBS for 4 h and then exposed to 100 µL dimethyl sulfoxide (DMSO; Sigma-Aldrich). Cell viability was measured by absorption at 570 nm in a microplate spectrophotometer

(Spectromax 250 plate reader). Results are shown as relative cell viability. MTT obtained values were normalized and concentrations transformed to logarithm, the nonlinear regression (curve fit) and IC_{50} were calculated using a log(geldanamycin) versus response algorithm.

In vivo geldanamycin treatment. Female BALB/cJAusb mice (10 – 12 weeks) were inoculated IP with 5 x 10^5 AB1-Luc on their right flank. Mice were randomly allocated to the different groups on the first treatment day. Initial mouse weight was measured immediately before the first geldanamycin injection, and it was used to calculate the amount to dose (5 mL/kg). Treatment with geldanamycin started on day 5 after tumour inoculation. Geldanamycin (1, 0.5 or 0.1 mg/kg) was prepared in sterile DMSO 1% and saline and dosed to all mice via a single intraperitoneal injection. Mice were dosed for a maximum of five consecutive days, twice a day (8 hours apart). In vivo imaging system (IVIS) (see below) was performed on days 4 (before treatment), 7 (during treatment) and 10 (after treatment). Mice were euthanized on day 10 once bioluminescence image was completed and in accordance with animal ethics guidelines and organs were harvested for staining.

In vivo imaging system (IVIS). XenoLight D-Luciferin potassium salt (PerkinElmer, VIC, Australia) was used at a 150 mg/kg concentration dissolved in sterile PBS. Approximately 150 µL (15 mg/mL concentration) was injected subcutaneously per mouse. Mice were anaesthetised in a chamber with a controlled flow of isoflurane 2% and oxygen flow rate of 1 L/min. When mice were fully unconscious, eye gel was applied to moisturise eyes during the imaging process. Mice were then transferred to the IVIS Lumina II camera chamber and isofluorane was decreased to 0.5 – 1% and oxygen flow rate to 0.8 L/min. Mice were imaged for 5 second exposure duration at 13 min post injection. Tumour burden is calculated as average radiance (photons/sec/cm^2/sr).

Hematoxylin and eosin staining. Mouse tissues were fixed with 4% paraformaldehyde for 48 - 72 hours and embedded in paraffin. 5 µm sections were cut by microtome (Thermo Fisher Scientific) and placed on Microscope Slides with 20 mm Colourfrost blue (Hurst Scientific). Slides were deparaffinised at room temperature as follows: 2 rounds of xylene (3 min each), 2 rounds of 100% ethanol (2 min

each), 95% ethanol (1 min), 70% ethanol (1 min), 40% ethanol (1 min), 3 rounds of distilled H_2O (3 min each). Slides were stained with Mayers hematoxylin (Sigma-Aldrich) for 10 min and rinsed with running tap water, the counterstain was performed with acidified Eosin Y solution (Sigma-Aldrich) (0.5% glacial acetic acid) for 45 seconds. Dehydration was performed as follows: 40% ethanol (30 sec), 70% ethanol (30 sec), 95% ethanol (30 sec), 2 rounds of 100% ethanol (1 min each), 2 rounds of xylene (3 min each). Mounting was performed with Pertex mounting medium (Histolab), and sections were imaged under a light microscope.

Quantification and statistical analysis

GraphPad Prism software was used to determine statistical significance of differences between groups by unpaired t-test when comparing two groups. A p value < 0.05 was considered significant. Each figure legend contains all the statistical details on each experiment, including the specific statistical test for that assay, exact value of n, what n represents and dispersion and precision measures. RNA sequencing statistical details can be found under Methods: RNA sequencing analysis.

Availability of data

The generated datasets used in this manuscript have been deposited at Gene Expression Omnibus (GEO) and are publicly available. Accession number is GSE180618. The rest of the relevant data are within the manuscript and its Supporting Information files.

ACKNOWLEDGEMENTS

Funding for this work was received from Cancel Council WA and iCare Dust Diseases Care. W.J.L. was funded by fellowships from the NHMRC, the Simon Lee Foundation and Cancer Council of Western Australia. M.L.O.M acknowledges the Commonwealth Government's support through the University Postgraduate Award and Australian Government Research Training Program Scholarships at The University of Western Australia. The authors also acknowledge the facilities and scientific and

technical assistance of the National Imaging Facility, a National Collaborative Research Infrastructure Strategy (NCRIS) capability, and Microscopy Australia at the Centre for Microscopy, Characterisation and Analysis, The University of Western Australia. A facility funded by the University, State and Commonwealth Governments.

REFERENCES

1. Kim J, Bhagwandin S, Labow DM. Malignant peritoneal mesothelioma: A review. Ann Transl Med. 2017;5(11):1–11.

2. Bibby AC, Tsim S, Kanellakis N, Ball H, Talbot DC, Blyth KG, et al. Malignant pleural mesothelioma: An update on investigation, diagnosis and treatment. Eur Respir Rev [Internet]. 2016;25(142):472–86. Available from: http://dx.doi.org/10.1183/16000617.0063-2016

3. Robinson BWS, Lake RA. Advances in Malignant Mesothelioma. N Engl J Med [Internet]. 2005;353(15):1591–603. Available from: http://www.nejm.org/doi/abs/10.1056/NEJMra050152

4. Odenthal J, Takes R, Friedl P. Plasticity of tumor cell invasion: Governance by growth factors and cytokines. Carcinogenesis. 2016;37(12):1117–28.

5. Friedl P, Alexander S. Cancer invasion and the microenvironment: Plasticity and reciprocity. Cell [Internet]. 2011;147(5):992–1009. Available from: http://dx.doi.org/10.1016/j.cell.2011.11.016

6. Vogelzang NJ, Rusthoven JJ, Symanowski J, Denham C, Kaukel E, Ruffie P, et al. Phase III study of pemetrexed in combination with cisplatin versus cisplatin alone in patients with malignant pleural mesothelioma. J Clin Oncol. 2003;21(14):2636–44.

7. Baas P, Scherpereel A, Nowak AK, Fujimoto N, Peters S, Tsao AS, et al. First-line nivolumab plus ipilimumab in unresectable malignant pleural mesothelioma (CheckMate 743): a multicentre, randomised, open-label, phase 3 trial. Lancet. 2021;397(10272):375–86.

8. Nowak AK, Lesterhuis WJ, Kok PS, Brown C, Hughes BG, Karikios DJ, et al. Durvalumab with first-line chemotherapy in previously untreated malignant pleural mesothelioma (DREAM): a multicentre, single-arm, phase 2 trial with a safety run-in. Lancet Oncol [Internet]. 2020;21(9):1213–23. Available from: http://dx.doi.org/10.1016/S1470-2045(20)30462-9

9. Kok PS, Forde PM, Hughes B, Sun Z, Brown C, Ramalingam S, et al. Protocol of DREAM3R: DuRvalumab with chEmotherapy as first-line treAtment in advanced pleural Mesothelioma-a phase 3 randomised trial. BMJ Open. 2022;12(1):1–8.

10. Iorio F, Rittman T, Ge H, Menden M, Saez-Rodriguez J. Transcriptional data: A new gateway to drug repositioning? Drug Discov Today [Internet]. 2013;18(7–8):350–7. Available from: http://dx.doi.org/10.1016/j.drudis.2012.07.014

11. Lamb J, Crawford ED, Peck D, Modell JW, Blat IC, Wrobel MJ, et al. The Connectivity Map: Using Gene-Expression Signatures to Connect Small Molecules, Genes, and Disease. Science (80-). 2006;313(5795):1929–35.

12. Duan Q, Reid SP, Clark NR, Wang Z, Fernandez NF, Rouillard AD, et al. L1000CDS2: LINCS L1000 characteristic direction signatures search engine. npj Syst Biol Appl [Internet]. 2016;2(16015):1–12. Available from: http://dx.doi.org/10.1038/npjsba.2016.15

13. Hurle MR, Yang L, Xie Q, Rajpal DK, Sanseau P, Agarwal P. Computational drug repositioning: From data to therapeutics. Clin Pharmacol Ther. 2013;93(4):335–41.

14. Orozco Morales ML, Rinaldi CA, de Jong E, Lansley SM, Gummer JPA, Olasz B, et al. PPARα and PPARγ activation is associated with pleural mesothelioma invasion but therapeutic inhibition is ineffective. iScience [Internet]. 2022;25(1):103571. Available from: https://doi.org/10.1016/j.isci.2021.103571

15. Love MI, Huber W, Anders S. Moderated estimation of fold change and dispersion for RNA-seq data with DESeq2. Genome Biol. 2014;15(550):1–21.

16. Krämer A, Green J, Pollard J, Tugendreich S. Causal analysis approaches in ingenuity pathway analysis. Bioinformatics. 2014;30(4):523–30.

17. Anderson CM, Hu J, Barnes RM, Heidt AB, Cornelissen I, Black BL. Myocyte enhancer factor 2C function in skeletal muscle is required for normal growth and glucose metabolism in mice. Skelet Muscle. 2015;5(1):1–10.

18. Zheng XL. Myocardin and smooth muscle differentiation. Arch Biochem Biophys [Internet]. 2014;543:48–56. Available from: http://dx.doi.org/10.1016/j.abb.2013.12.015

19. Lynn DJ, Winsor GL, Chan C, Richard N, Laird MR, Barsky A, et al. InnateDB: Facilitating systems-level analyses of the mammalian innate immune response. Mol Syst Biol. 2008;4(218).

20. Mootha VK, Lindgren CM, Eriksson K-F, Subramanian A, Sihag S, Lehar J, et al. PGC-1α-responsive genes involved in oxidative phosphorylation are coordinately downregulated in human diabetes. Nat Genet. 2003;34(3):267–73.

21. Subramanian A, Tamayo P, Mootha VK, Mukherjee S, Ebert BL, Gillette MA, et al. Gene set enrichment analysis: A knowledge-based approach for interpreting genome-wide expression profiles. Proc Natl Acad Sci U S A. 2005;102(43):15545–50.

22. Ashburner M, Ball CA, Blake JA, Botstein D, Bulter H, Cherry JM, et al. Gene Ontology: tool for the unification of biology. Nat Genet [Internet]. 2000;25:25–9. Available from: http://www.ncbi.nlm.nih.gov/pubmed/10802651

23. Liberzon A, Birger C, Thorvaldsdóttir H, Ghandi M, Mesirov JP, Tamayo P. The Molecular Signatures Database (MSigDB) hallmark gene set collection. Cell Syst. 2016;1(6):417–25.

24. Chen EY, Tan CM, Kou Y, Duan Q, Wang Z, Meirelles G V., et al. Enrichr: Interactive and collaborative HTML5 gene list enrichment analysis tool. BMC Bioinformatics. 2013;14.

25. Kuleshov M V., Jones MR, Rouillard AD, Fernandez NF, Duan Q, Wang Z, et al. Enrichr: a comprehensive gene set enrichment analysis web server 2016 update. Nucleic Acids Res. 2016;44(1):W90–7.

26. Xie Z, Bailey A, Kuleshov M V., Clarke DJB, Evangelista JE, Jenkins SL, et al. Gene Set Knowledge Discovery with Enrichr. Curr Protoc. 2021;1(3):1–51.

27. Whitesell L, Mimnaugh EG, De Costa B, Myers CE, Neckers LM. Inhibition of heat shock protein HSP90-pp60(v-src) heteroprotein complex formation by benzoquinone ansamycins: Essential role for stress proteins in oncogenic transformation. Proc Natl Acad Sci U S A. 1994;91(18):8324–8.

28. Neckers L, Schulte TW, Mimnaugh E. Geldanamycin as a potential anti-cancer agent: Its molecular target and biochemical activity. Invest New Drugs. 1999;17(4):361–73.

29. Yun BG, Matts RL. Differential effects of Hsp90 inhibition on protein kinases regulating signal transduction pathways required for myoblast differentiation. Exp Cell Res. 2005;307(1):212–23.

30. Wagatsuma A, Shiozuka M, Kotake N, Takayuki K, Yusuke H, Mabuchi K, et al. Pharmacological inhibition of HSP90 activity negatively modulates myogenic differentiation and cell survival in C2C12 cells. Mol Cell Biochem. 2011;358(1–2):265–80.

31. Chai K, Ning X, Nguyn TTT, Zhong B, Morinaga T, Li Z, et al. Heat shock protein 90 inhibitors augment endogenous wild-type p53 expression but down-regulate the adenovirally-induced expression by inhibiting a proteasome activity. Oncotarget. 2018;9(40):26130–43.

32. Sohn EJ. Bioinformatic Analysis of Potential Biomarker for hsa-miR-196b-5p in Mesothelioma. Genet Test Mol Biomarkers [Internet]. 2021;25(12):772–80. Available from: https://www.liebertpub.com/doi/epub/10.1089/gtmb.2021.0147#

33. Bucci M, Roviezzo F, Cicala C, Sessa WC, Cirino G. Geldanamycin, an inhibitor of heat shock protein 90 (Hsp90) mediated signal transduction has anti-inflammatory effects and interacts with glucocorticoid receptor in vivo. Br J Pharmacol. 2000;131:13–6.

34. Hassan R, Kindler HL, Jahan T, Bazhenova L, Reck M, Thomas A, et al. Phase II clinical trial of amatuximab, a chimeric antimesothelin antibody with pemetrexed and cisplatin in advanced unresectable pleural mesothelioma. Clin Cancer Res. 2014;20(23):5927–36.

35. Hassan R, Sharon E, Thomas A, Zhang J, Ling A, Miettinen M, et al. Phase 1 study of the antimesothelin immunotoxin SS1P in combination with pemetrexed and cisplatin for front-line therapy of pleural mesothelioma and correlation of tumor response with serum mesothelin, megakaryocyte potentiating factor, and cancer antigen. Cancer. 2014;120(21):3311–9.

36. Servais EL, Colovos C, Rodriguez L, Bograd AJ, Nitadori JI, Sima C, et al. Mesothelin overexpression promotes mesothelioma cell invasion and MMP-9 secretion in an orthotopic mouse model and in epithelioid pleural mesothelioma patients. Clin Cancer Res. 2012;18(9):2478–89.

37. He X, Wang L, Riedel H, Wang K, Yang Y, Dinu CZ, et al. Mesothelin promotes epithelial-to-mesenchymal transition and tumorigenicity of human lung cancer and mesothelioma cells. Mol Cancer. 2017;16(63):1–13.

38. Zucali PA, Simonelli M, De Vincenzo F, Fatuzzo G, Bertossi M, Suter MB, et al. Phase I-Ib trial of tivantinib in combination with carboplatin and pemetrexed as first-line treatment in patients (pts) with advanced nonsquamous NSCLC or malignant pleural mesothelioma (MPM). J Clin Oncol [Internet]. 2014;32(15):suppl, TPS7610-TPS7610. Available from: https://ascopubs.org/doi/abs/10.1200/jco.2014.32.15_suppl.tps7610

39. Thayaparan T, Spicer JF, Maher J. The role of the HGF/Met axis in mesothelioma. Biochem Soc Trans. 2016;44(2):363–70.

40. Pon JR, Marra MA. MEF2 transcription factors: developmental regulators and emerging cancer genes. Oncotarget. 2015;7(3).

41. Homminga I, Pieters R, Langerak AW, de Rooi JJ, Stubbs A, Verstegen M, et al. Integrated Transcript and Genome Analyses Reveal NKX2-1 and MEF2C as Potential Oncogenes in T Cell Acute Lymphoblastic Leukemia. Cancer Cell [Internet]. 2011;19(4):484–97. Available from:

http://dx.doi.org/10.1016/j.ccr.2011.02.008

42. Schwieger M, Schüler A, Forster M, Engelmann A, Arnold MA, Delwel R, et al. Homing and invasiveness of MLL/ENL leukemic cells is regulated by MEF2C. Blood. 2009;114(12):2476–88.

43. Bai X, Wu L, Liang T, Liu Z, Li J, Li D, et al. Overexpression of myocyte enhancer factor 2 and histone hyperacetylation in hepatocellular carcinoma. J Cancer Res Clin Oncol. 2008;134(1):83–91.

44. Zhang JJ, Zhu Y, Xie KL, Peng YP, Tao JQ, Tang J, et al. Yin Yang-1 suppresses invasion and metastasis of pancreatic ductal adenocarcinoma by downregulating MMP10 in a MUC4/ErbB2/p38/MEF2C-dependent mechanism. Mol Cancer. 2014;13(130):1–17.

45. Miano JM. Myocardin in biology and disease. J Biomed Res. 2015;29(December 2014):3–19.

46. Medjkane S, Perez-Sanchez C, Gaggioli C, Sahai E, Treisman R. Myocardin-related transcription factors and SRF are required for cytoskeletal dynamics and experimental metastasis. Nat Cell Biol. 2009;11(3):257–68.

47. Datta A, Deng S, Gopal V, Yap KCH, Halim CE, Lye ML, et al. Cytoskeletal dynamics in epithelial-mesenchymal transition: Insights into therapeutic targets for cancer metastasis. Cancers (Basel). 2021;13(1882):1–27.

48. He W, Wu L, Gao Q, Du Y, Wang Y. Identification of AHBA biosynthetic genes related to geldanamycin biosynthesis in Streptomyces hygroscopicus 17997. Curr Microbiol. 2006;52(3):197–203.

49. Fukuyo Y, Hunt CR, Horikoshi N. Geldanamycin and its anti-cancer activities. Cancer Lett [Internet]. 2010;290(1):24–35. Available from: http://dx.doi.org/10.1016/j.canlet.2009.07.010

50. Lee EJ. Cancer Chemoprevention Effects of Geldanamycin and 17-AAG in Human Oral Squamous Cell Carcinoma. Korean J Clin Lab Sci. 2018;50(4):462–9.

51. Alqawi O, Moghaddas M, Singh G. Effects of geldanamycin on HIF-1α mediated angiogenesis and invasion in prostate cancer cells. Prostate Cancer Prostatic Dis. 2006;9(2):126–35.

52. Okamoto J, Mikami I, Tominaga Y, Kuchenbecker KM, Lin YC, Bravo DT, et al. Inhibition of Hsp90 leads to cell cycle arrest and apoptosis in human malignant pleural mesothelioma. J Thorac Oncol [Internet]. 2008;3(10):1089–95. Available from: http://dx.doi.org/10.1097/JTO.0b013e3181839693

53. Tran AA, Prasad V. Drug repurposing for cancer treatments: a well-intentioned, but misguided strategy. Lancet Oncol. 2020;21(9):1134–6.

54. Hernández-Lemus E, Martínez-García M. Pathway-Based Drug-Repurposing Schemes in Cancer: The Role of Translational Bioinformatics. Front Oncol. 2021;10(January):1–15.

55. Begley CG, Ashton M, Baell J, Bettess M, Brown MP, Carter B, et al. Drug repurposing: Misconceptions, challenges, and opportunities for academic researchers. Sci Transl Med. 2021;13(612):1–13.

56. Jackaman C, Bundell CS, Kinnear BF, Smith AM, Filion P, van Hagen D, et al. IL-2 Intratumoral Immunotherapy Enhances CD8 + T Cells That Mediate Destruction of Tumor Cells and Tumor-Associated Vasculature: A Novel Mechanism for IL-2 . J Immunol. 2003;171(10):5051–63.

57. Davis MR, Manning LS, Whitaker D, Garlepp MJ, Robinson BWS. Establishment of a murine model of malignant mesothelioma. Int J Cancer. 1992;52(6):881–6.

58. Fear VS, Forbes CA, Chee J, Ma S, Neeve S, Celliers L, et al. Neo-antigen specific T cell responses indicate the presence of metastases before imaging. Sci Rep. 2019;9(1):1–10.

59. Manning LS, Whitaker D, Murch AR, Garlepp MJ, Davis MR, Musk AW, et al. Establishment and characterization of five human malignant mesothelioma cell lines derived from pleural effusions. Int J Cancer. 1991;47(2):285–90.

60. Lansley SM, Cheah HM, Della Vergiliana JFV, Chakera A, Lee YCG. Tissue plasminogen activator potently stimulates pleural effusion via a monocyte chemotactic protein-1-dependent mechanism. Am J Respir Cell Mol Biol. 2015;53(1):105–12.

61. Bray NL, Pimentel H, Melsted P, Pachter L. Near-optimal probabilistic RNA-seq quantification. Nat Biotechnol. 2016;34(5):525–7.

62. Breuer K, Foroushani AK, Laird MR, Chen C, Sribnaia A, Lo R, et al. InnateDB: Systems biology of innate immunity and beyond - Recent updates and continuing curation. Nucleic Acids Res. 2013;41(D1):1228–33.

63. Horibata S, Vo T V., Subramanian V, Thompson PR, Coonrod SA. Utilization of the Soft Agar Colony Formation Assay to Identify Inhibitors of Tumorigenicity in Breast Cancer Cells. J Vis Exp [Internet]. 2015;99(e52727):1–7. Available from: http://www.jove.com/video/52727/utilization-soft-agar-colony-formation-assay-to-identify-inhibitors

SUPPLEMENTARY DATA

Supplementary Fig S1. Geldanamycin causes weight loss when dosed at 1 or 0.5 mg/kg *in vivo* (A) Mice weight monitored daily during treatment at 1 mg/kg, each dotted line indicates the number of doses. (B) Mice weight monitored daily during treatment at 0.5 mg/kg, each doted like indicates two doses on that specific day.

Supplementary Table S1. Mice clinical signs scoring criteria

Score		0	1	2
Appearance	*Weight Loss*	Steady weight	>10% weight loss	15%-19.99% weight loss
	Coat	Normal	Mild ruffled coat	Moderate ruffled coat, ungroomed
	Body Condition	Normal	Thin	Loss of body fat, failure to grow
	Body Posture	Normal	Hunched	Hunched and still
	Movement	Normal	Reduced/slow	Reluctant to move when touched
Activity	*Proximity to Others*	Normal	Somewhat separate	Completely separate
Other	*Injection Site*	Normal	Some redness at margins	Redness and

515 **Supplementary Table S2.** Mice intervention criteria

Score	Assessment	Intervention
0	Animal normal	No intervention needed. Standard monitoring procedure.
1	Animal slightly deviated from normal	Increase monitoring to 3x weekly. The animal will be monitored again within 24 hours if a score above zero is recorded.
2	Animal demonstrates mild deviation from normal	Increase monitoring to daily until animal returns to normal
3-4	Animal demonstrates moderate deviation from normal	Monitor 2x daily, weigh 3x a week. Contact Bioresources staff for advice or administer pain relief (Buprenorphine). Consider euthanasia.
>4	Animal demonstrates significant deviation from normal or is noticeably distressed or unwell	Euthanasia

516

517 **Supplementary Data S1. LINCS and CMap results** Excel file (.xlsx): AB1 and AE17 pleural differentially expressed genes.

518

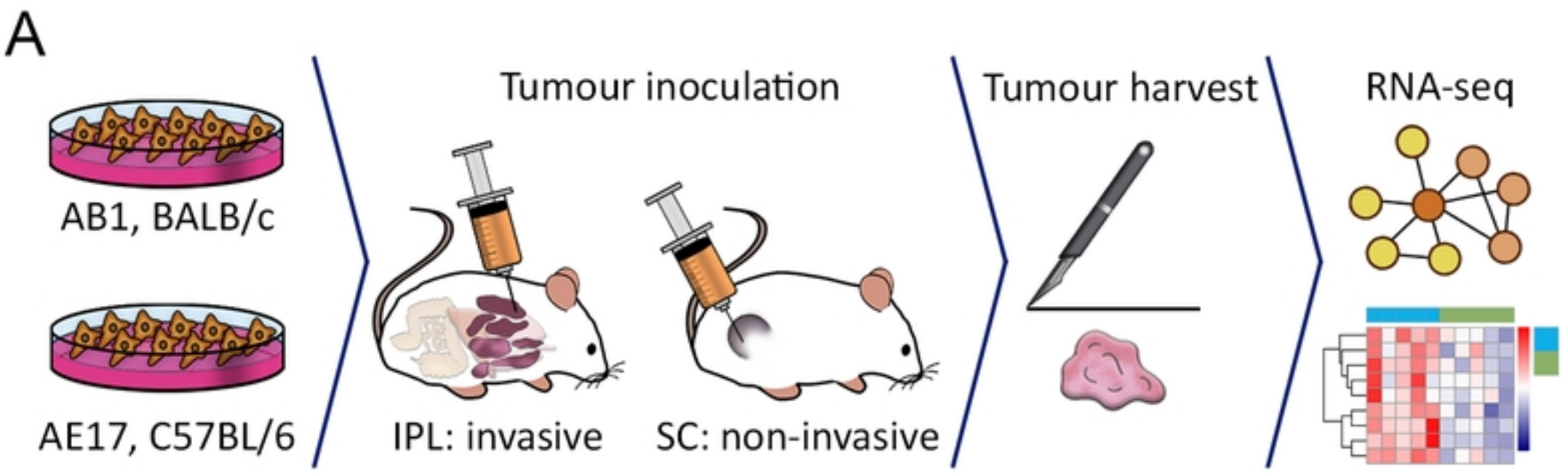

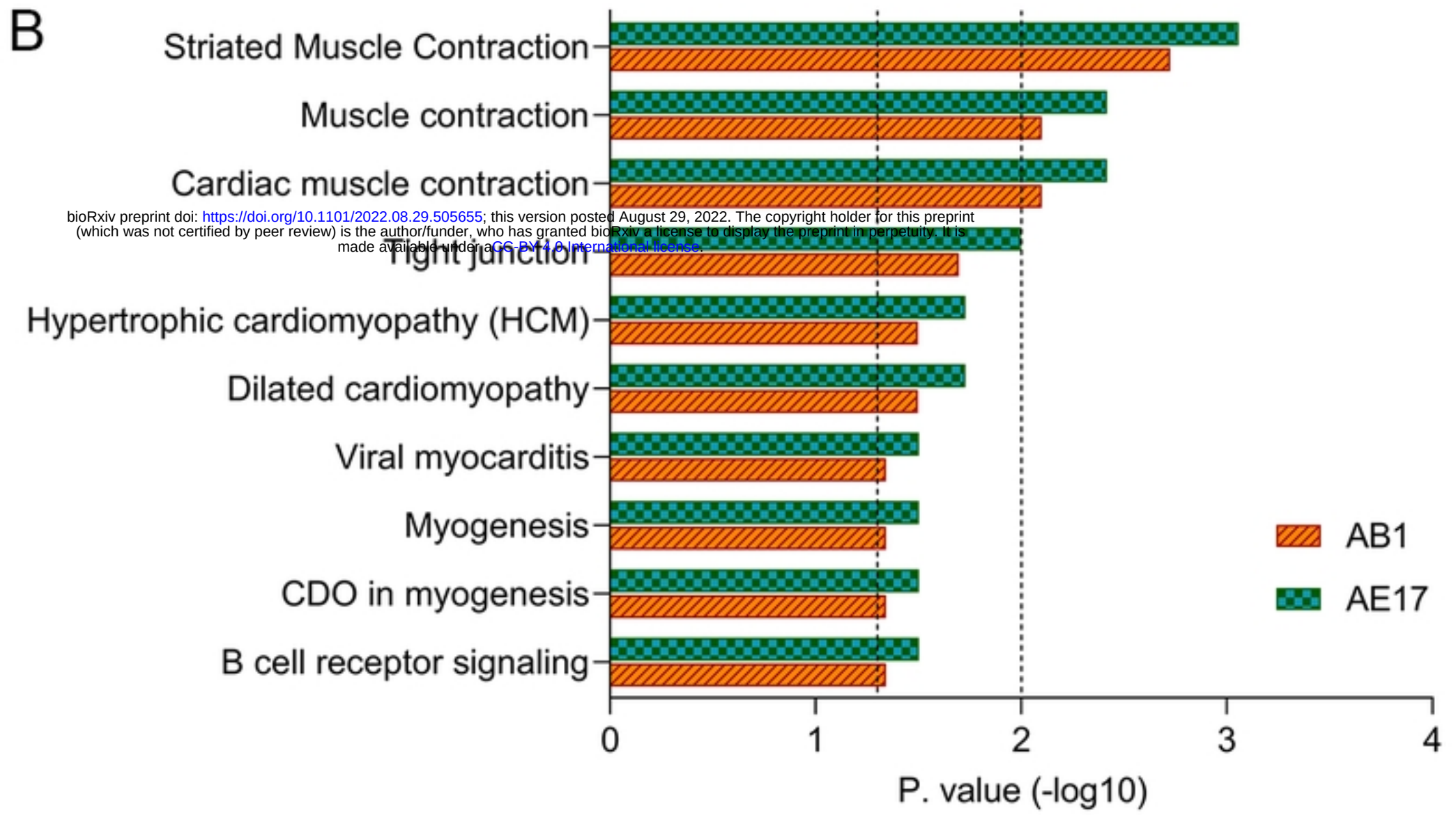

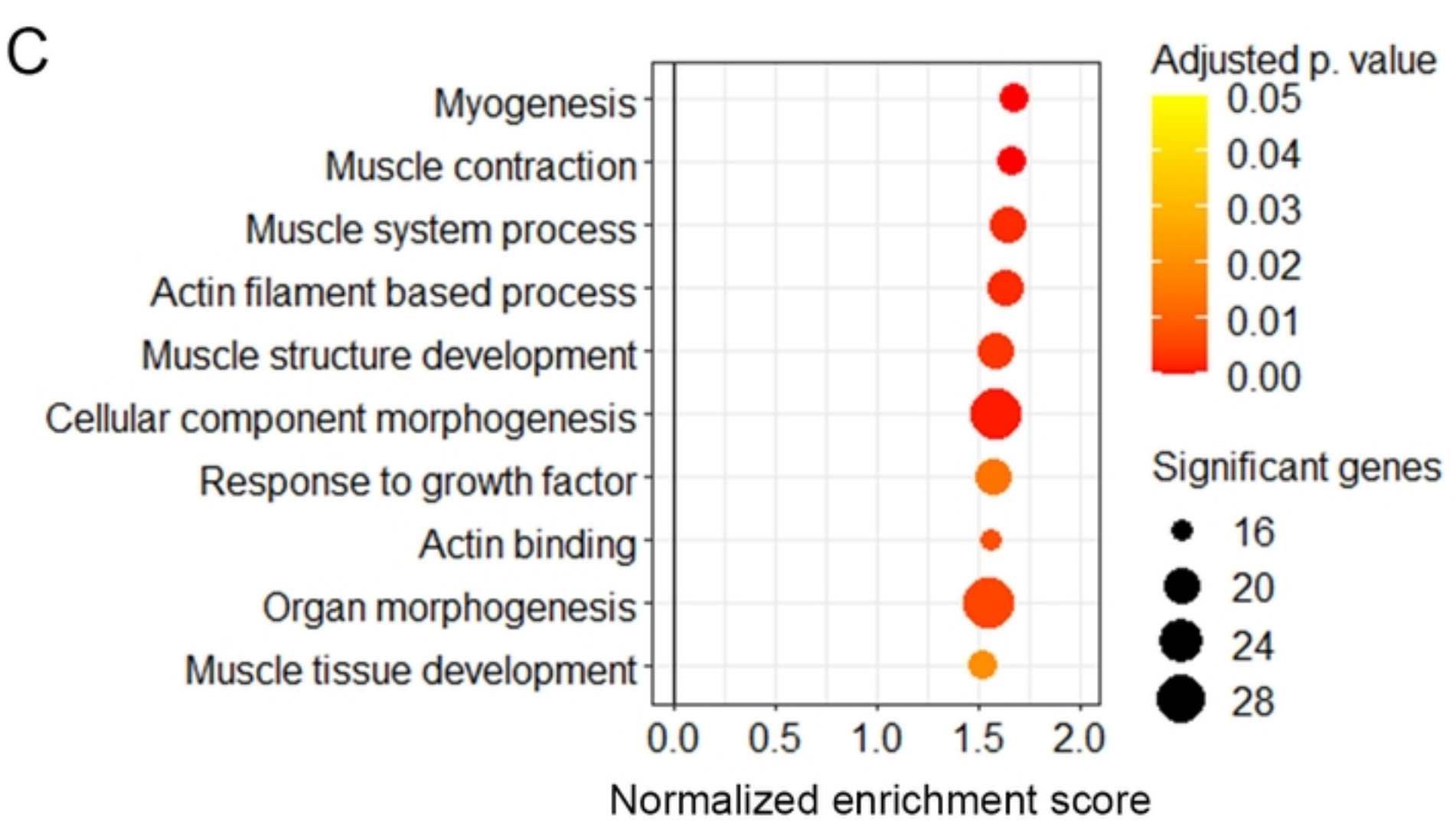

Figure1

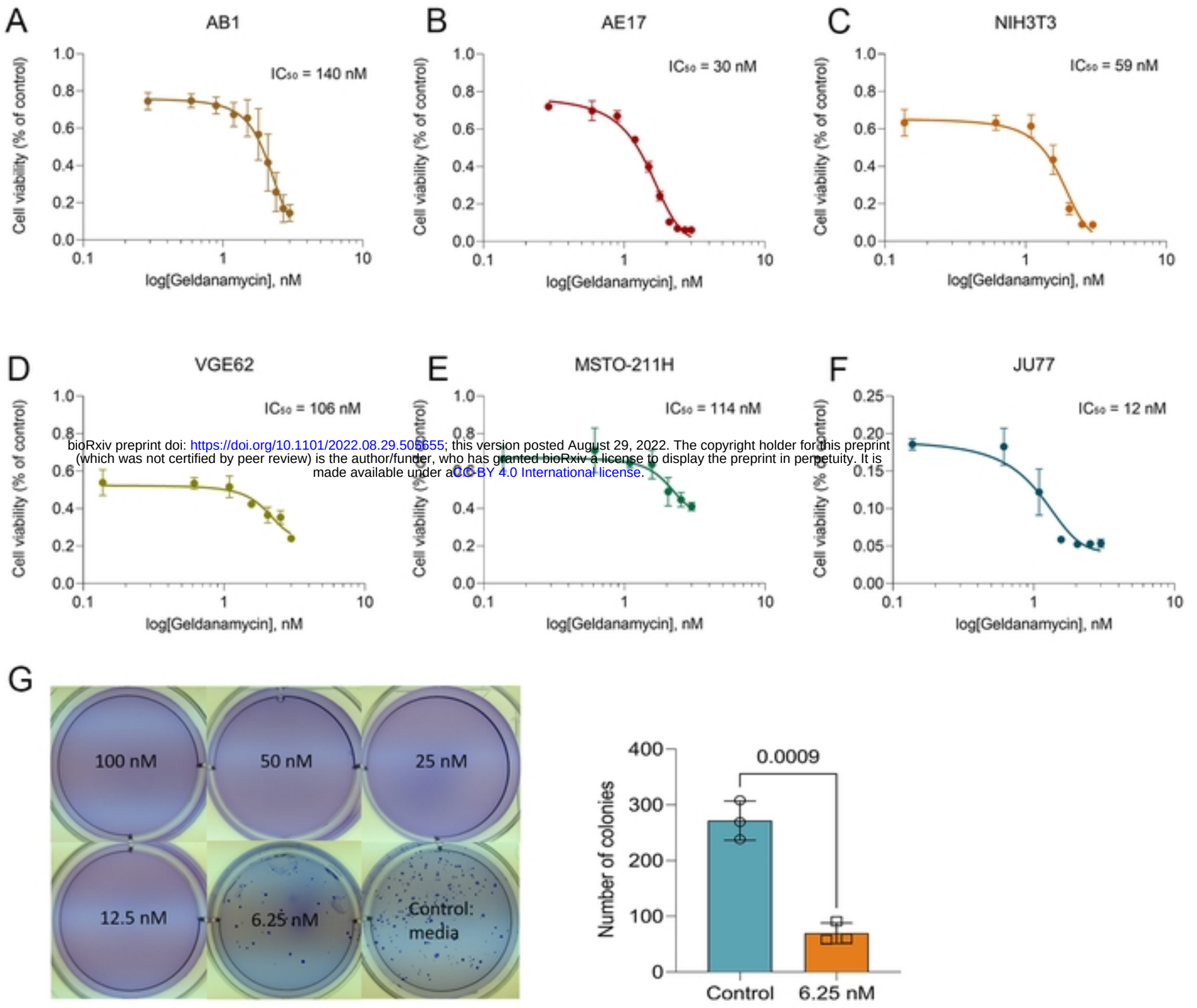

Figure 2

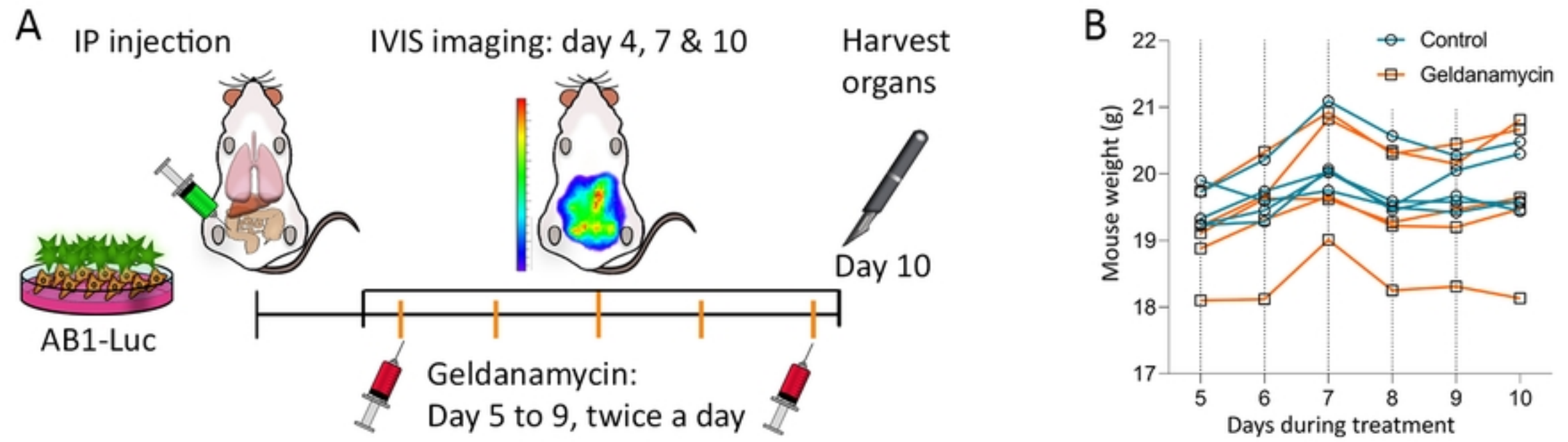

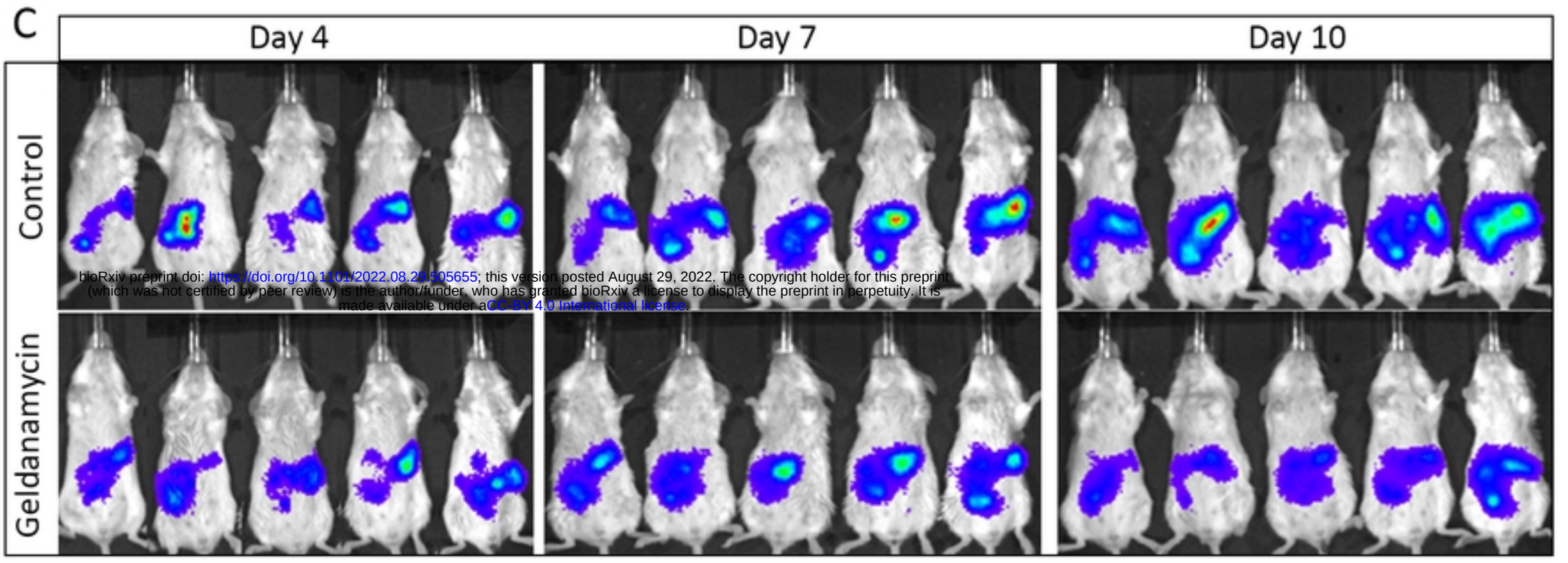

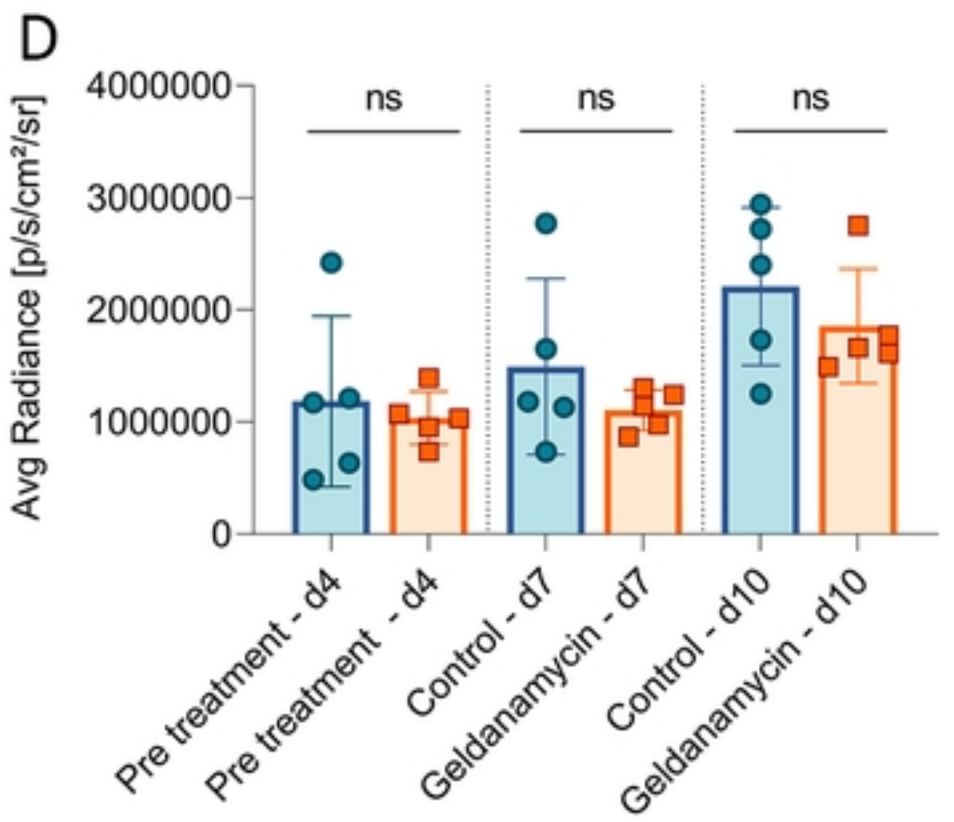

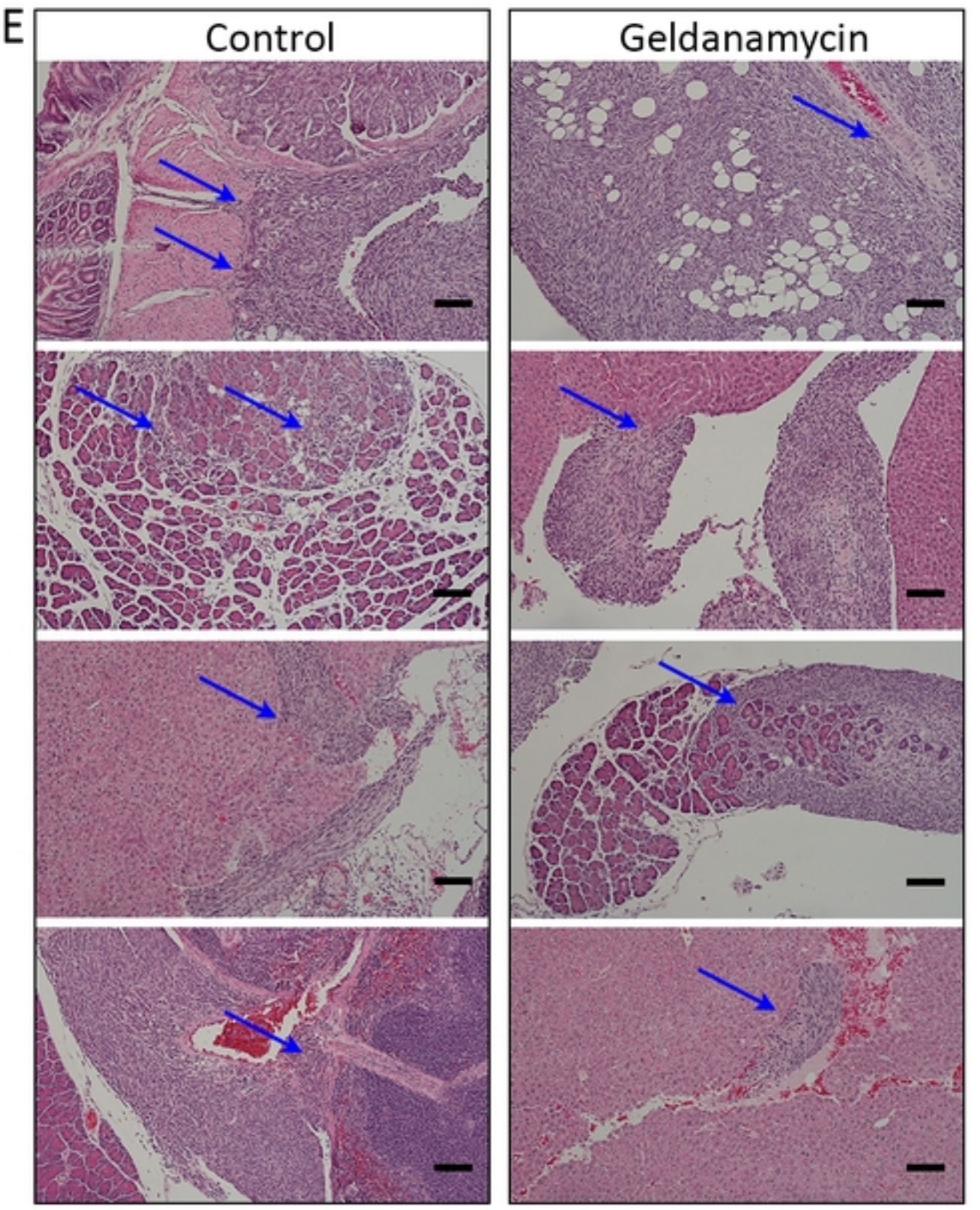

Figure 3